corrosion and materials degradation

MDPI

Article

Diffusion Potentials in Cement Mortars with pH Differences Due to Carbonation

Elke Ziehensack *, Kai Osterminski and Christoph Gehlen

Centre for Building Materials, Technical University of Munich, Franz-Langinger-Straße 10, 81245 Munich, Germany
* Correspondence: elke.ziehensack@tum.de

Abstract: Corrosion investigations of steel-reinforced concrete structures are often based on half-cell potential measurements, in which the diffusion potentials can be a significant source of measurement errors. Therefore, the diffusion potentials must be taken into account in order to enable accurate half-cell potential measurements. This study covers the measurement of the diffusion potentials in cement mortars with pH differences due to carbonation and various mortar moisture conditions. The effect of chloride exposure of the mortars on the diffusion potentials is outside of the scope of this study. The mortars consisted of ordinary Portland cement (OPC) and blast furnace cement (BFC) with water–cement ratios of 0.5–0.7. The use of color indicators allows for the observation of the pH drop around the carbonation front, which propagates as the carbonation progresses. The diffusion potentials in the mortars under study have measurement values between 10 and 240 mV. The measured diffusion potentials seem to correlate with the magnitude of the pH drop rather than the progress of the carbonation depth. The moisture condition of the mortars significantly affects the magnitude of the arising diffusion potentials.

Keywords: diffusion potential; concrete; pH; moisture; carbonation; half-cell potential measurement; measurement error; experimental setup

Academic Editor: Miguel-Ángel Climent

Received: 30 October 2024
Revised: 4 December 2024
Accepted: 16 December 2024
Published: 24 December 2024

Citation: Ziehensack, E.; Osterminski, K.; Gehlen, C. Diffusion Potentials in Cement Mortars with pH Differences Due to Carbonation. *Corros. Mater. Degrad.* **2025**, *6*, 2. https://doi.org/10.3390/cmd6010002

1. Introduction

Corrosion significantly reduces the service life of steel-reinforced concrete structures. Corrosion-related investigations often rely on measuring the half-cell potential of the steel reinforcement embedded in concrete (Figure 1).

Half-cell potential measurements indicate whether the steel is in a passive or active (depassivated) state [1]. Half-cell potential mapping has become an established inspection method to locate actively corroding steel areas in reinforced concrete structures [1,2]. In monitoring systems, half-cell potential measurements have been used to detect corrosion onset and to study the corrosion behavior of the steel embedded in concrete [3–8]. However, phenomena in concrete such as the diffusion potentials may significantly interfere with the measured half-cell potentials [9–14]. Therefore, the diffusion potentials must be taken into account when measuring the half-cell potentials. Diffusion potentials occur whenever there are differences in the concentration of the ions in a concrete pore solution owing to their different mobilities (compare with [9,10]).

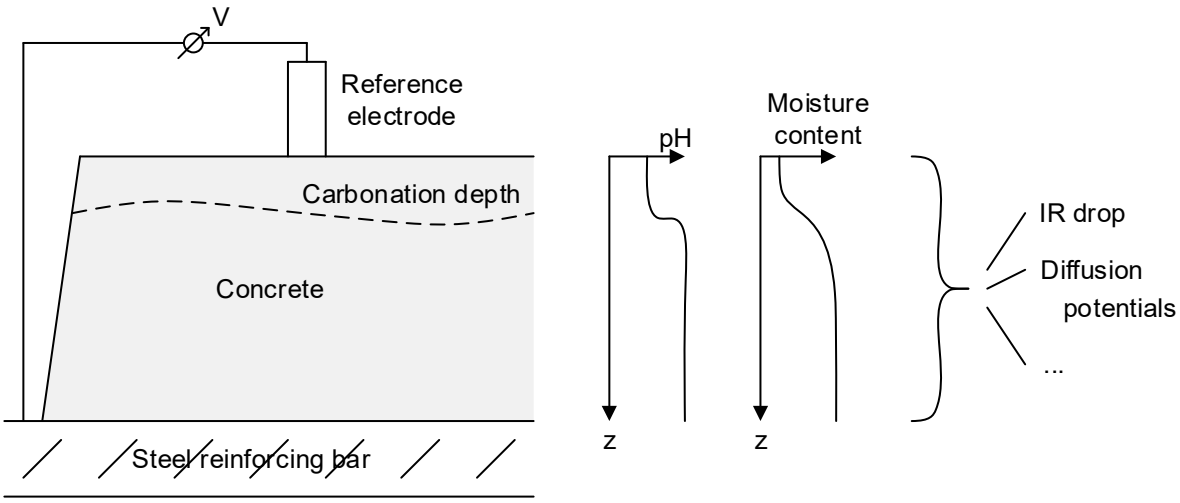

Figure 1. Measurement of the half-cell potential of the steel reinforcement embedded in concrete.

An estimation of the diffusion potentials can, under some conditions, be made when using the Henderson equation [11,15] (Equation (1) from [16]).

$$E_D = \frac{RT}{F} \frac{\sum u_i \frac{|z_i|}{z_i} (c_{2,i} - c_{1,i})}{\sum u_i |z_i| (c_{2,i} - c_{1,i})} \ln \frac{\sum u_i |z_i| c_{1,i}}{\sum u_i |z_i| c_{2,i}} \quad (1)$$

$c_{1,i}$ and $c_{2,i}$ denote the spatially different ion concentrations, u_i is the ion mobility of the species i, z_i is the ion charge valence of the species i, T is the temperature, R is the ideal gas constant, and F is the Faraday constant. For the calculations, the following have to be known: exact pore solution compositions, ion concentration profiles, ion mobilities of the involved species in concrete, etc. Another option is to determine the diffusion potentials by measurements.

Several authors [9–12] found that pH differences in the concrete pore solution had a major influence on the arising diffusion potentials, which were expected to be about 30 mV per pH unit [9]. If reinforced concrete structures are not submerged in water, pH differences of 3–6 units [17–23] result from the carbonation of concrete. The associated diffusion potentials are estimated to be 90–180 mV, which may act as a significant source of measurement error. In the literature [9–12,24], however, the diffusion potentials have mostly been studied in solution experiments. There is a lack of data for the diffusion potentials in cement-based materials with pH differences due to carbonation.

The aim of this study is to improve the current understanding of the diffusion potentials that arise in cement-based materials under atmospheric conditions. The focus is on studying the diffusion potentials in cement mortars with pH differences due to carbonation and various mortar moisture conditions including saturation with water. The effect of chloride exposure of the mortars on the diffusion potentials is outside of the scope of this study.

Furthermore, the experimental setup for measuring the diffusion potentials is introduced. The advantages and limitations of this measurement setup are discussed.

2. Materials and Methods

Figure 2 gives an overview of the study of the diffusion potentials in cement mortars with pH differences and various mortar moisture conditions.

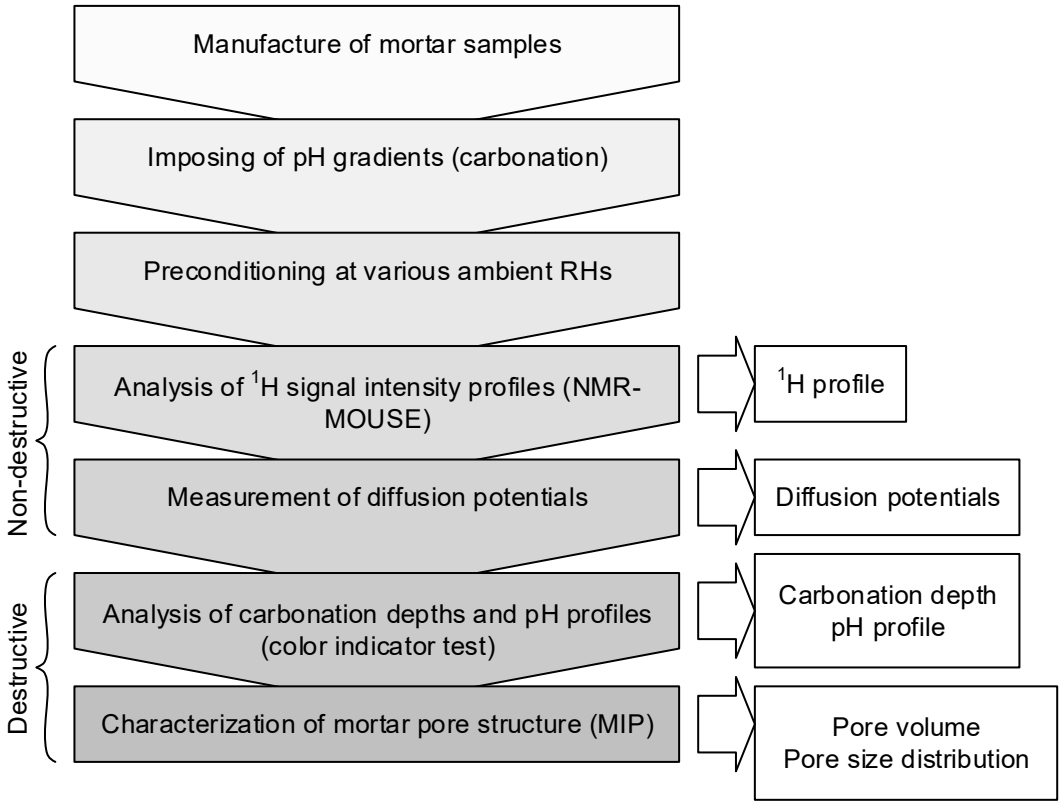

Figure 2. Schematic illustration of the study of the diffusion potentials in cement mortars with pH differences and various mortar moisture conditions.

2.1. Manufacture of Mortar Samples

This study focused on ordinary Portland cement (OPC) and blast furnace cement (BFC) mortars with water–cement (w/c) ratios of 0.5 and 0.7, see Table 1. While a w/c ratio of 0.5 has commonly been used in practice, the w/c ratio of 0.7 was chosen to accelerate the carbonation progress of the mortar made of OPC due to its relatively high carbonation resistance (high Portlandite buffer capacities [25]). The chemical compositions of the cements can be found in [26]. Sand, in accordance with DIN EN 196-1 [27], with a maximum grain size of 2 mm was used. The volume of the sand was 58%, which was kept equal for every mortar mixture. Cylindrical mortar samples were manufactured, which had a diameter of 46 mm and a length of usually 20–25 mm. The mortars were cured at room temperature while being left in an airtight casting mold for over 56 d.

Table 1. Mix proportions (by weight) of the cement mortars under study.

	Cement Mortar		
	OPC-0.5	**OPC-0.7**	**BFC-0.5**
Cement			
OPC	1.00	1.00	-
BFC	-	-	1.00
Water	0.50	0.70	0.50
Sand	3.00	3.73	3.00

2.2. Imposing of pH Gradients (Carbonation)

At the age of 56 d, carbonation of the mortars started, based on DIN EN 12390-12 [28]. This included the preconditioning at room temperature and a relative humidity of around 60% (average) over two weeks and the subsequent storage of the mortars in

a carbonation chamber with a temperature of 20 °C, a relative humidity (RH) of 57%, and a CO_2 concentration of 3 vol.-% (accelerated carbonation (ACC)). The samples were stored in the carbonation chamber for up to 376 d, which allowed us to study the diffusion potentials at various carbonation depths. During carbonation, an aluminum tape sealed the sample surfaces, except for the frontal surface, to form a one-dimensional CO_2 transport.

2.3. Preconditioning at Various Ambient RHs

After carbonation, the mortar samples were stored at various ambient relative humidities over periods of two weeks and three months to equilibrate the moisture conditions. Relative humidities of 65, 85, 95 and 98% were chosen, which allowed us to study the influence of mortar moisture conditions. Considering the capillary pores (>10–50 nm [29,30]), pore sizes > 10 nm were expected to be free of water at 65 and 85% RHs, while pore sizes up to 21 and 53 nm were assumed to be filled with water at 95 and 98% RHs, respectively (compare with [31]). The different relative humidities were set at approx. 20 °C with the help of saturated salt solutions or aqueous glycerin solutions at the bottom of airtight containers. The aqueous glycerin solutions had glycerin contents of 68 and 20 wt.-% to set 65 and 95% RHs, respectively. A saturated KCl solution and a saturated K_2SO_4 solution were used to set 85 and 98% RHs, respectively. During preconditioning, the carbonated mortar surfaces had a distance of at least 5 cm, while the opposite uncarbonated mortar surfaces were covered with foil. After storage at 85% RH, an additional series of samples were immersed in tap water to a depth of 1–2 mm with the carbonated surface facing downwards for 1 d. The relative humidity of 85% was chosen to ensure the capillary pores were free of water prior to the immersion. At the end of the immersion, the excess water was removed from the sample surface with a paper towel.

2.4. Analysis of ^1H Signal Intensity Profiles

The ^1H signal intensity profiles of the mortars were investigated via the ^1H nuclear magnetic resonance mobile universal surface explorer (NMR-MOUSE) from Magritek, which is non-destructive test equipment. This method has proven to be suitable for the investigation of spatial ^1H distributions in cement-based materials [32–34].

A Profile NMR-MOUSE PM 25 including a high precision lift and a Kea spectrometer were used [35]. A spacer with a thickness of 15 mm was installed. Each mortar sample was placed on a microscope slide made of glass (thickness = 1.1 mm) in the magnetic field of a permanent magnet. An RF coil was used (operating frequency = 13.49 MHz) to excite the hydrogen nuclei in the sensitive volume (length × width × height = 3 cm × 3 cm × 500 µm) at a certain depth within the sample and receive the signal by applying the Carr–Purcell–Meiboom–Gill (CPMG) pulse sequence. The number of echoes was 256, the number of scans was 250 with a repetition time of 1000 ms. The initial signal was taken, which usually had the maximum intensity correlating with the amount of water in the examined volume at a certain depth in the mortar sample. The NMR-MOUSE signals were corrected by shifting the phase angle for which the imaginary part becomes zero using Equations (2) and (3).

$$Re(\varphi) = A \cdot \cos\varphi \tag{2}$$

$$Im(\varphi) = A \cdot \sin\varphi \tag{3}$$

Re and *Im* denote the real and imaginary part of the signal, A is the amplitude, and φ is the phase angle.

The measurements were executed at various depths by moving the lift to obtain a ^1H signal intensity profile along the sample depth. As the measurements were re-

stricted to a maximum sample depth of 8.5 mm, the carbonated and opposite uncarbonated near-surface areas of each mortar sample were investigated. During measurement, the mortar samples were covered with foil (thickness = 0.01 mm) to prevent changes in their moisture conditions.

2.5. Measurement of Diffusion Potentials

The diffusion potential measurements were executed on a series of three samples for each carbonation depth and moisture condition at a temperature of approx. 20 °C. Figure 3 shows the diffusion potential measurement setup, which was used in this study. The measurements were executed by means of a high impedance voltmeter (impedance $\geq$ 2.6 GOhm [36]) and a pair of reference electrodes. The reference electrode (RE) was a silver chloride electrode with an inner electrolyte, which consisted of saturated potassium chloride. The two reference electrodes were coupled to the carbonated and opposite uncarbonated mortar surfaces with the help of a coupling agent on cellulosic filter paper. The RE, which was coupled to the carbonated mortar surface, was connected to the minus pole of the voltmeter. The measurement setup was covered with foil to prevent changes in the moisture condition of the mortar under study. Stable potential readings were taken, i.e., changes in the measurement curve over time were $\leq$1 mV/min. The potential readings were corrected by the residual RE potential difference. Since two reference electrodes of the same type were used, the residual RE potential difference was <0.3 mV, which was subtracted.

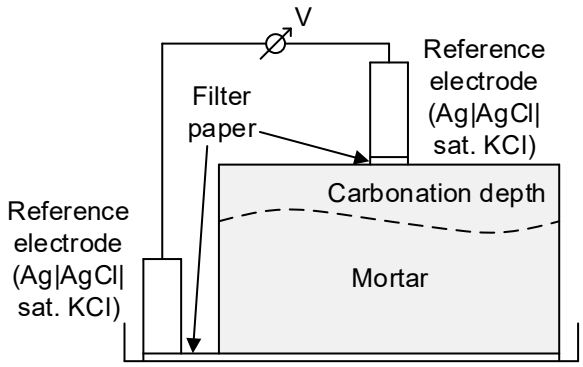

Figure 3. Diffusion potential measurement setup.

For the RE coupling, various coupling agents were considered. One option was to couple the two reference electrodes to the uncarbonated and carbonated mortar surfaces with a synthetic pore solution and tap water, respectively (case 1). Table 2 lists the synthetic pore solution compositions, which were chosen based on the compositions of the expressed pore solutions published in [26]. The synthetic pore solutions were prepared using deionized water. No $Ca(OH)_2$ was added to the synthetic pore solutions, as this would have promoted rapid carbonation during RE coupling, which would have impaired the stability of the diffusion potential measurements. The composition of the tap water can be found in [37]. In this case, the chemical compositions of the coupling agents were similar to those of the pore solutions near the un-/carbonated mortar surfaces. Another option was to use a saturated KCl solution for the coupling of the reference electrodes to both the uncarbonated and carbonated mortar surfaces (case 2). A KCl solution has commonly been used as salt bridge electrolyte in electrochemistry experiments [38]. In this case, the coupling agent was identical to the inner electrolyte of the RE. Both cases enabled us to keep additional diffusion potentials due to the coupling of RE to the mortar surfaces at small values of <3.5 mV (estimated with Equation (1)). This minimized interference with the potential readings.

Table 2. Compositions of the synthetic pore solutions used for RE coupling.

	Content [g/L]		pH *
	NaOH	**KOH**	
OPC-0.5	3.18	17.87	13.5
OPC-0.7	2.01	11.27	13.3
BFC-0.5	2.51	10.57	13.3

* Measurement with pH meter.

2.6. Analysis of Carbonation Depths and pH Profiles

After executing the diffusion potential measurements, the use of destructive testing methods completed the investigations. In order to visualize the carbonation depths and the pH profiles in the mortars, color indicators were chosen. Other methods have been discussed controversially [18,19,39].

Figure 4 shows the carbonation depth (left) and pH profile (right) present in a BFC-0.5 mortar sample. A thymolphthalein indicator was used (with color changes at pH 9.4–10.6 [40]) to determine the carbonation depth based on DIN EN 12390-12 [28]. The thymolphthalein indicator solution was prepared by adding 0.1 g of thymolphthalein to 100 mL of ethanol. Furthermore, a commercially available rainbow indicator with color changes at several points was used (from Germann Instruments; blue at pH 12–14, violet at pH 10–12, green at pH 8–10, yellow at pH 6–8, and orange at pH 4–6 [41]). The rainbow indicator was shown to be suitable for determining pH profiles in cement-based materials [42–44].

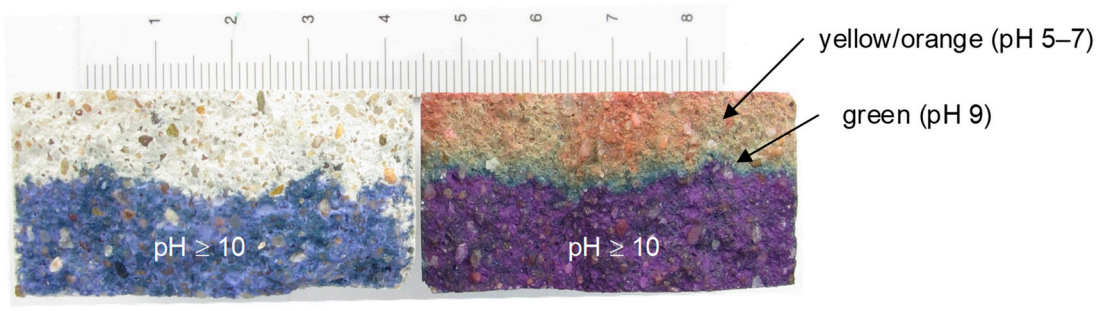

Figure 4. Analysis of carbonation depth via thymolphthalein indicator (**left**) and pH profile via rainbow indicator (**right**) for a BFC-0.5 mortar sample (cropped image and the original image is attached; see Supplementary Materials).

Immediately after splitting the mortar samples along their longitudinal axis, the thymolphthalein and rainbow indicators were applied to one of the split sample surfaces, respectively. Usually 1–3 h after application, the carbonation depth was measured at 5 mm intervals via a caliper.

2.7. Characterization of the Mortar Pore Structure

The pore structure was analyzed by mercury intrusion porosimetry (MIP) before and with the progressing carbonation of the mortars. The carbonated part of the mortar sample, which was visualized with the thymolphthalein indicator, was gained by sawing without the use of water. The uncarbonated mortar at the age of two months was taken as a reference.

3. Results and Discussion

3.1. pH Profiles Due to Carbonation of the Mortars

Figure 5 shows the progressing carbonation of the mortars, visualized with the rainbow indicator. The OPC-0.7 and BFC-0.5 mortars show a sudden drop in pH around the carbonation front, which propagates as the carbonation progresses. The pH drops from 13 to 14 [26] by approx. seven for both the OPC-0.7 and BFC-0.5 mortars. For the OPC-0.5 mortar, not only is the carbonation progression much slower but also the pH decrease is smaller. The reason for this could presumably be attributed to higher pH buffer capacities.

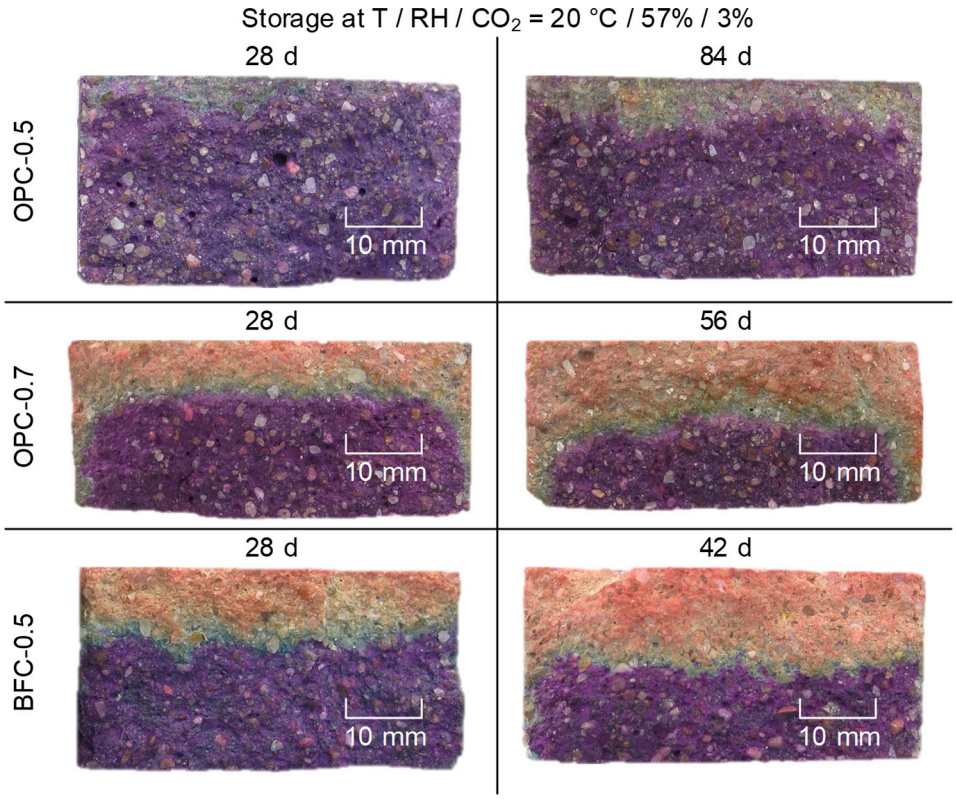

Figure 5. Progressing carbonation of the mortars; visualization with the rainbow indicator (grouping of cropped images and the original images are attached; see Supplementary Materials).

In the literature [18–20], the pH decreased to values around seven as a minimum, which resulted from the analysis of the pore solutions expressed from carbonated concrete/mortar. A slower pH decrease could be found with higher OPC contents [18,19]. These findings support the results of this study in Figure 5.

- A drop in pH around the carbonation front propagates with the progressing carbonation.

3.2. Pore Structure of the Mortars

Figure 6 shows the changes in the pore size distribution due to carbonation. This figure additionally plots the cumulative pore volume and, at its maximum, the mortar porosity. For all the mortars under study, there is a decrease in porosity, which results from carbonation. The reason for this is the formation of calcium carbonate ($CaCO_3$), which is associated with a reduction of the pore volume [25]. Compared to the OPC-0.5 mortar, the uncarbonated BFC-0.5 mortar has finer pore sizes, which shift towards larger values with the progressing carbonation. Despite the increased pore sizes in the carbonated BFC-0.5 mortar, there is a reduction in the porosity, which is in accordance with the literature [45].

- The pore structures considerably change as a result of carbonation.

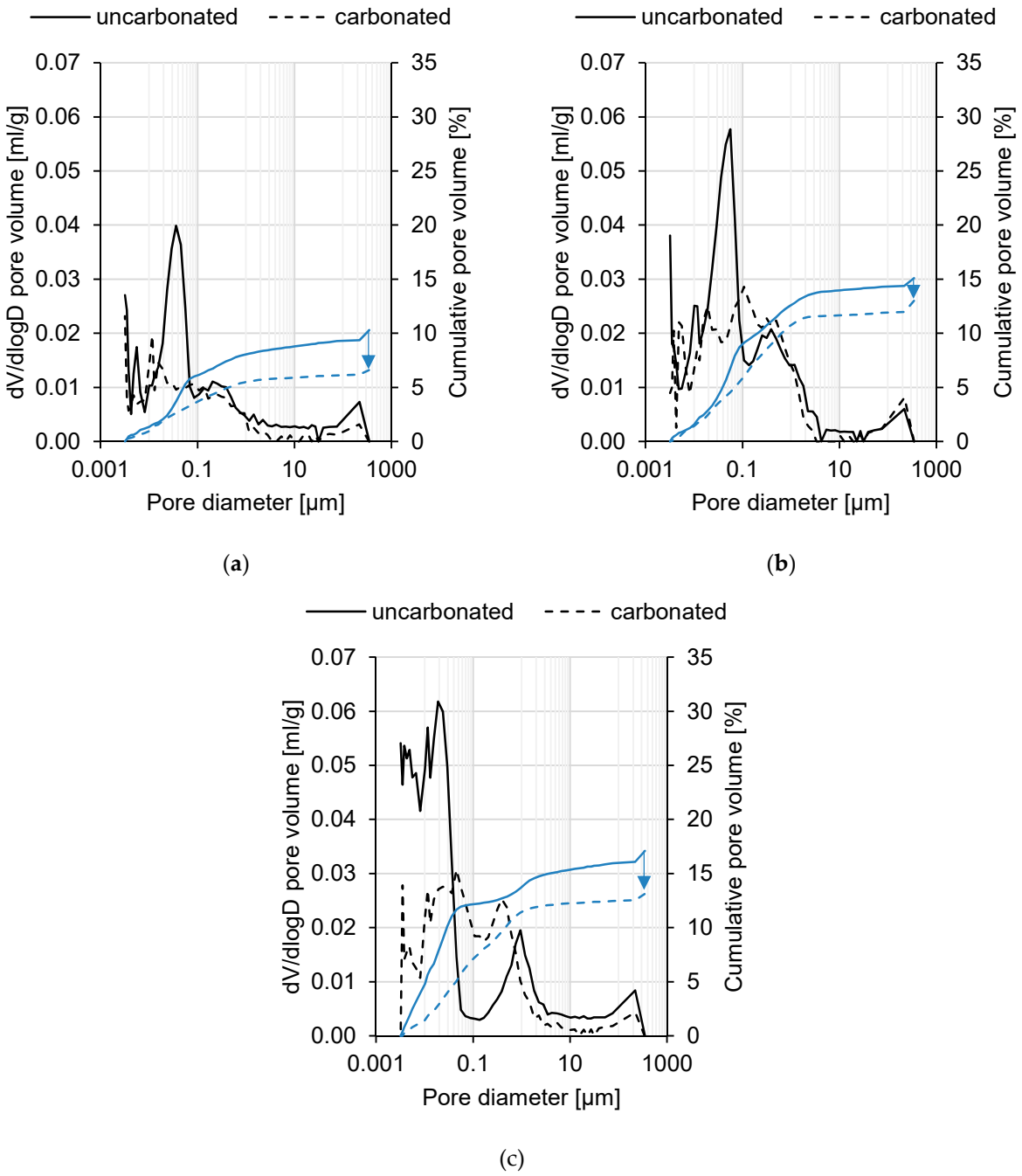

Figure 6. Changes in pore structure of the (**a**) OPC-0.5, (**b**) OPC-0.7, and (**c**) BFC-0.5 mortars due to carbonation; dV/dlogD pore volume (black) and cumulative pore volume (blue).

3.3. ^{1}H Signal Intensity Profiles in the Mortars

Figure 7 shows the ^{1}H signal intensity profiles in the mortars as the carbonation progresses. This figure plots the ^{1}H signal intensity as a function of the sample depth. Considerable differences in the signal intensities are found between the carbonated and uncarbonated areas within the mortar samples rather than due to the preconditioning at different relative humidities. The signal intensities in the carbonated areas are smaller when compared to the uncarbonated areas. The reason for this could be that the moisture uptake is less pronounced while preconditioning the samples at 65 and 98% RHs after storage in the carbonation chamber at a (smaller) RH of 57%. Another reason could be the reduced pore volume in the carbonated area, which is associated with a decrease in the water content and thus the ^{1}H signal intensity. The decrease in signal intensity seems to

propagate with progressing carbonation. Furthermore, there could be an effect due to the presence of OH^- at a high pH which is associated with a reduction in the ^1H signal intensity, which is estimated to be <1%.

- The differences in the ^1H signal intensity occur between the carbonated and uncarbonated mortar areas.

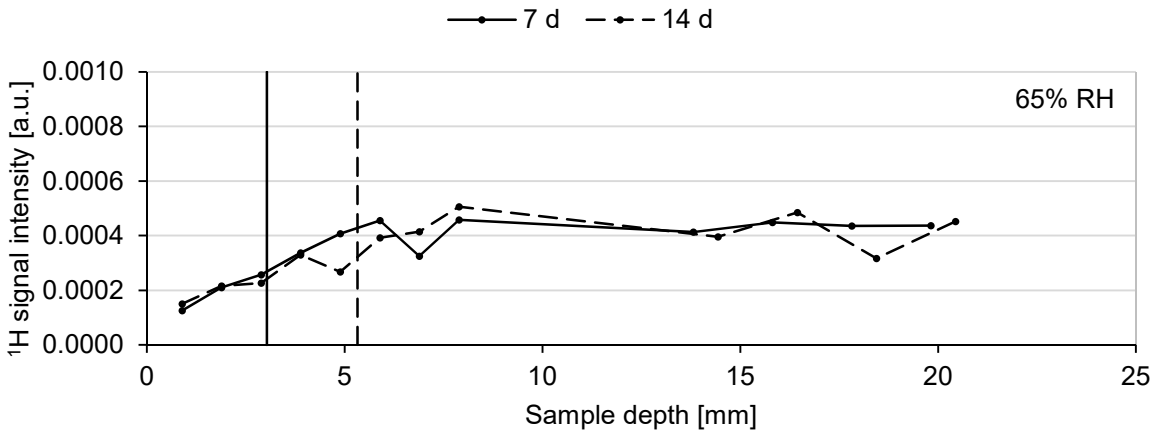

(**a**)

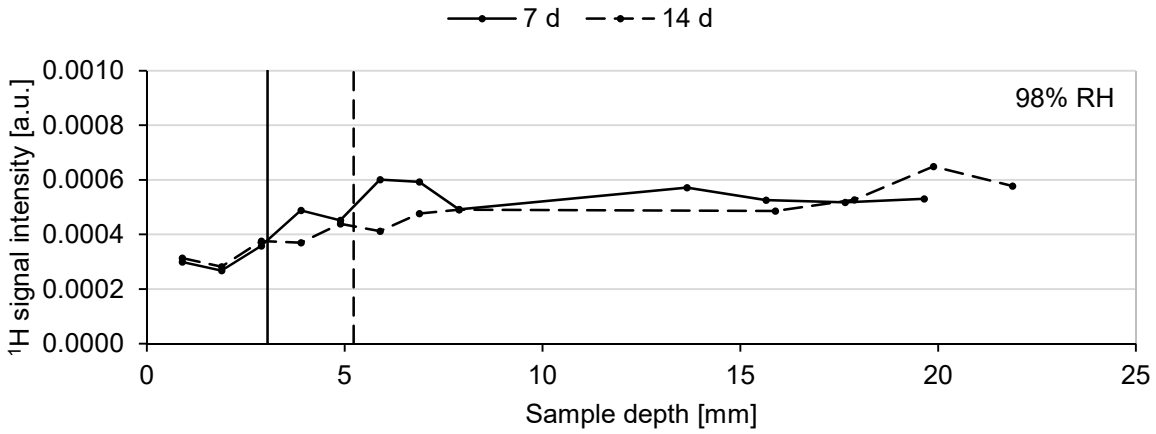

(**b**)

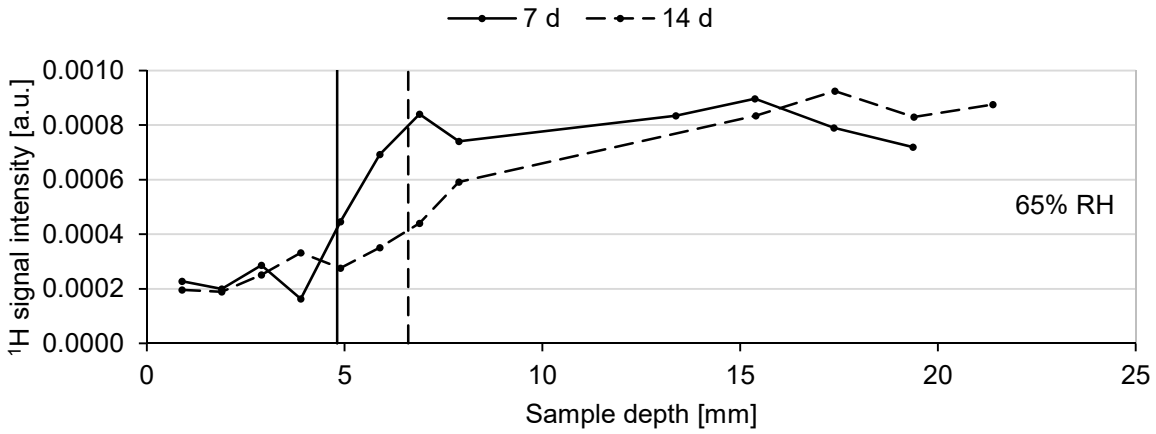

(**c**)

Figure 7. *Cont.*

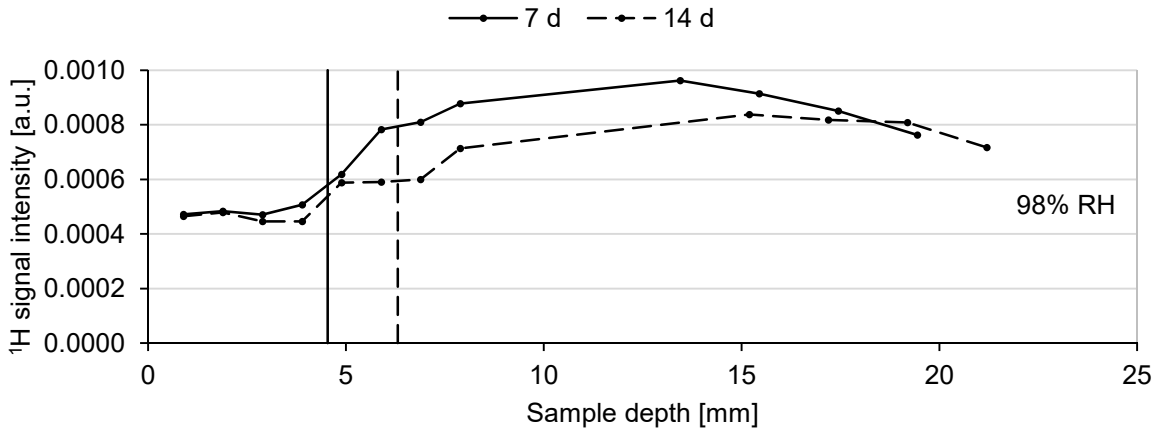

(**d**)

Figure 7. ^{1}H signal intensity profiles in the (**a**,**b**) OPC-0.7 and (**c**,**d**) BFC-0.5 mortars for 7 and 14 d ACC (preconditioning at 65 and 98% RHs over two weeks), and the associated carbonation depths (vertical line).

3.4. Diffusion Potentials in the Mortars

Figure 8 plots the diffusion potentials as a function of the carbonation depths, which was determined via the thymolphthalein indicator, for the mortars under study. This figure shows the measured diffusion potentials in the mortars after preconditioning at various ambient RHs over two weeks, and saturation with water. The diffusion potentials were measured using the measurement setup in Figure 3. For each measurement, the two reference electrodes were coupled to the uncarbonated and carbonated mortar surfaces with the help of a synthetic pore solution and tap water, respectively (case 1, see Section 2.5).

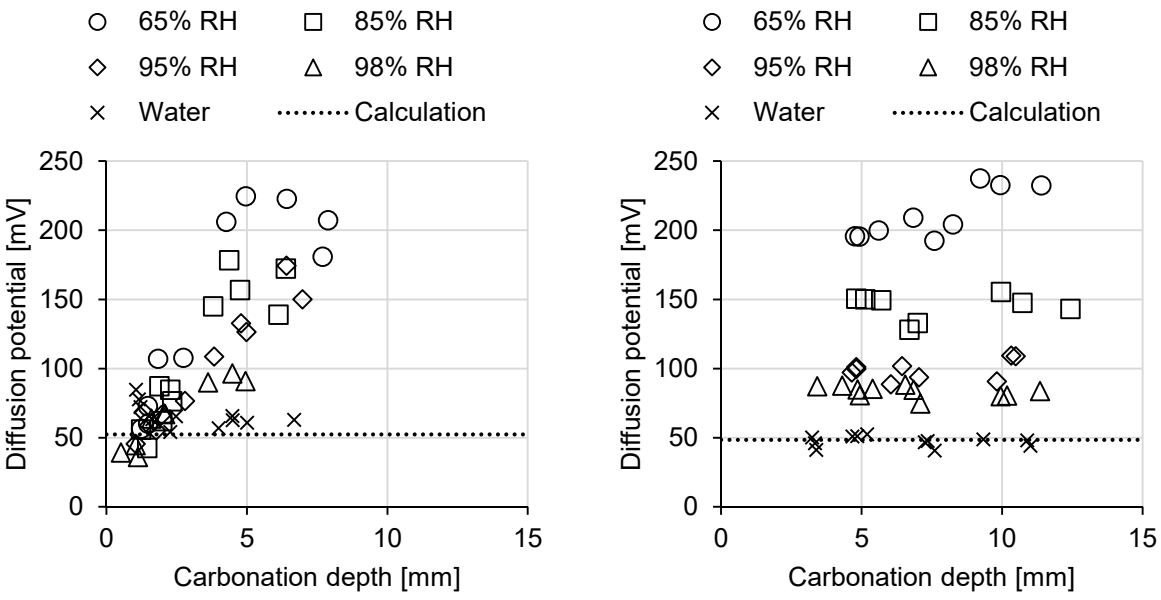

(**a**) (**b**)

Figure 8. *Cont.*

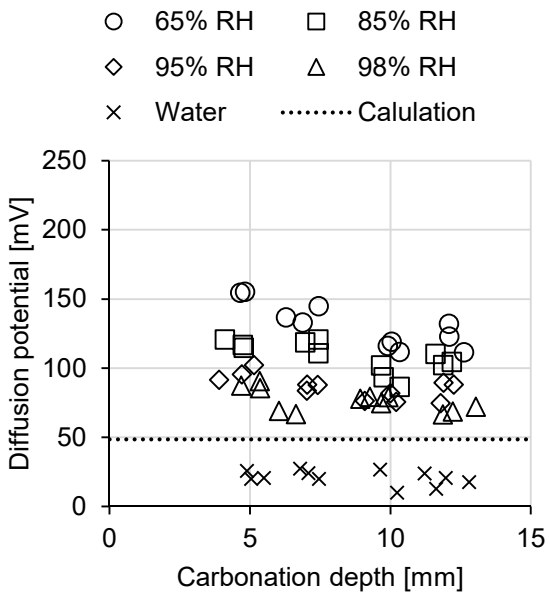

(**c**)

Figure 8. Diffusion potentials as a function of the carbonation depths for the (**a**) OPC-0.5, (**b**) OPC-0.7, and (**c**) BFC-0.5 mortars after preconditioning at various ambient RHs over two weeks, and saturation with water.

The diffusion potentials in the OPC mortars have measurement values of up to 240 mV, while the values are not higher than 160 mV for the BFC-0.5 mortar. Although carbonation is progressing, the diffusion potentials at carbonation depths > 3–4 mm approach certain values depending on the moisture conditions of the mortars. The diffusion potentials are smaller with a higher ambient RH, and the smallest measurement values occur in the case of water saturation. At small carbonation depths (<3–4 mm), the diffusion potentials increase with the progressing carbonation, and the effect of the moisture condition is not as pronounced. In the saturated mortar, the diffusion potentials usually measure around 20–65 mV, which agrees well with the values of around 30–60 mV for the various concrete mixtures in [24].

The stagnation of the diffusion potentials can be clearly seen at carbonation depths > 3–4 mm in the OPC-0.7 and BFC-0.5 mortars, for which the carbonation progresses at apparently constant pH differences (see Figure 5). For the OPC-0.5 mortar, more data are needed at the high carbonation depths. At the small carbonation depths < 3–4 mm in the OPC-0.5 mortar, the increase of the diffusion potentials may result from the dropping pH, i.e., the increasing pH difference. This suggests that the diffusion potentials seem to correlate with the magnitude of the pH drop rather than the progress of the carbonation depth.

The contribution of the pH differences to the measured diffusion potentials is studied with help of calculations using Equation (1). The calculations of the diffusion potentials that result from the pH differences in the pore solution allow for a comparison with the measured diffusion potentials under saturated conditions. When saturating the mortars with tap water, it is expected that the pH of the pore solution in the uncarbonated area buffers at high levels, while the pH remains decreased in the carbonated area, i.e., approx. pH 9 for the OPC-0.5 mortar and approx. pH 7 for the OPC-0.7 and BFC-0.5 mortars (see Section 3.1). Thus, one could think of an additional junction between the carbonated and uncarbonated pore solutions within the mortar (dashed line), as shown in Figure 9.

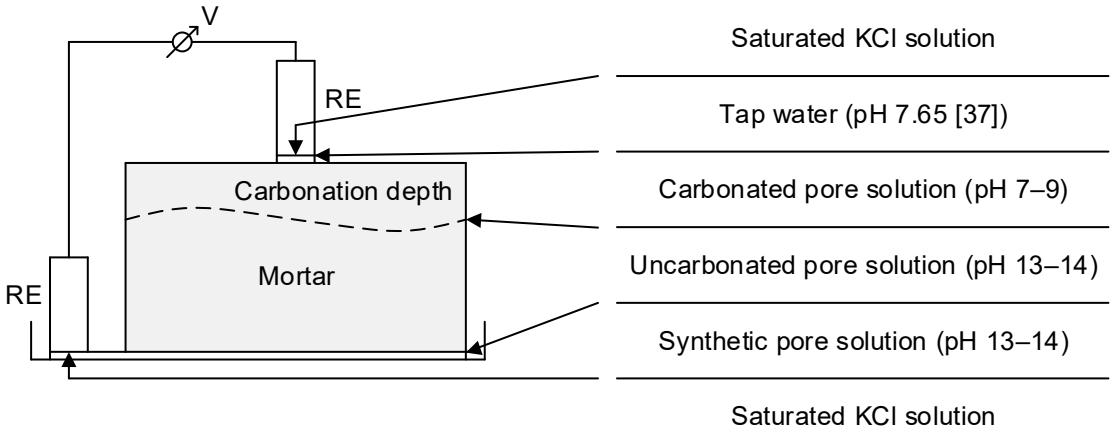

Figure 9. Liquid junctions assumed for the calculations of the diffusion potentials under saturated conditions.

The diffusion potential calculations are based on the ion mobilities in the solutions, and the assumption that the composition of the pore solution in the carbonated area is similar to tap water, which has the above pH values of 7–9. The calculations agree well with the measured diffusion potentials in the OPC mortars, see Figure 8. The agreement at carbonation depths < 2 mm in the OPC-0.5 mortar is less good owing to the higher level of scattering of the measured diffusion potentials. For the BFC-0.5 mortar, however, the comparability of the calculations with the measurements is poor. This could possibly be attributed to interactions with the pore walls and the ions present in the pore solution, which may affect the resulting diffusion potentials (permselective behavior, compare with [26]).

The increase of the diffusion potentials with the decreasing ambient RHs supports the finding in [12]. A possible explanation for this could be as follows. Under decreased moisture conditions, only the smaller pores are filled with the pore solution, which forces the diffusing hydroxyl ions and co-diffusing cations (Ca^{2+}, Na^{+}, K^{+}, etc.) closer to the pore walls (compare with [13]). Therefore, the effect of the pore wall interactions is expected to be more pronounced. The pore wall interactions would result in a reduction in the ion mobilities, which is presumably more pronounced for the cations than for the hydroxyl ion at the usually negatively charged pore walls (compare with [13,26]). This would increase the magnitude of the arising diffusion potentials. Further research is required to confirm this.

As it takes quite some time to equilibrate the mortar moisture conditions, a comparison of the different conditioning periods shows their influence on the resulting diffusion potentials. Figure 10 plots the measured diffusion potentials in the mortars after preconditioning at various relative humidities over the periods of two weeks and three months. The diffusion potential values are in a similar range for most of the mortars and relative humidities under study. As shown above, the diffusion potentials decrease with the increasing ambient RH, even though the mortar moisture conditions may not be fully equilibrated. This shows a minor influence of the chosen preconditioning periods on the resulting diffusion potentials in this study.

- The diffusion potentials seem to correlate with the size of the pH drop rather than the progress of the carbonation depth.
- The mortar moisture condition significantly affects the magnitude of the diffusion potentials. The lower the ambient RH, the higher the diffusion potentials. The preconditioning period has a minor influence.

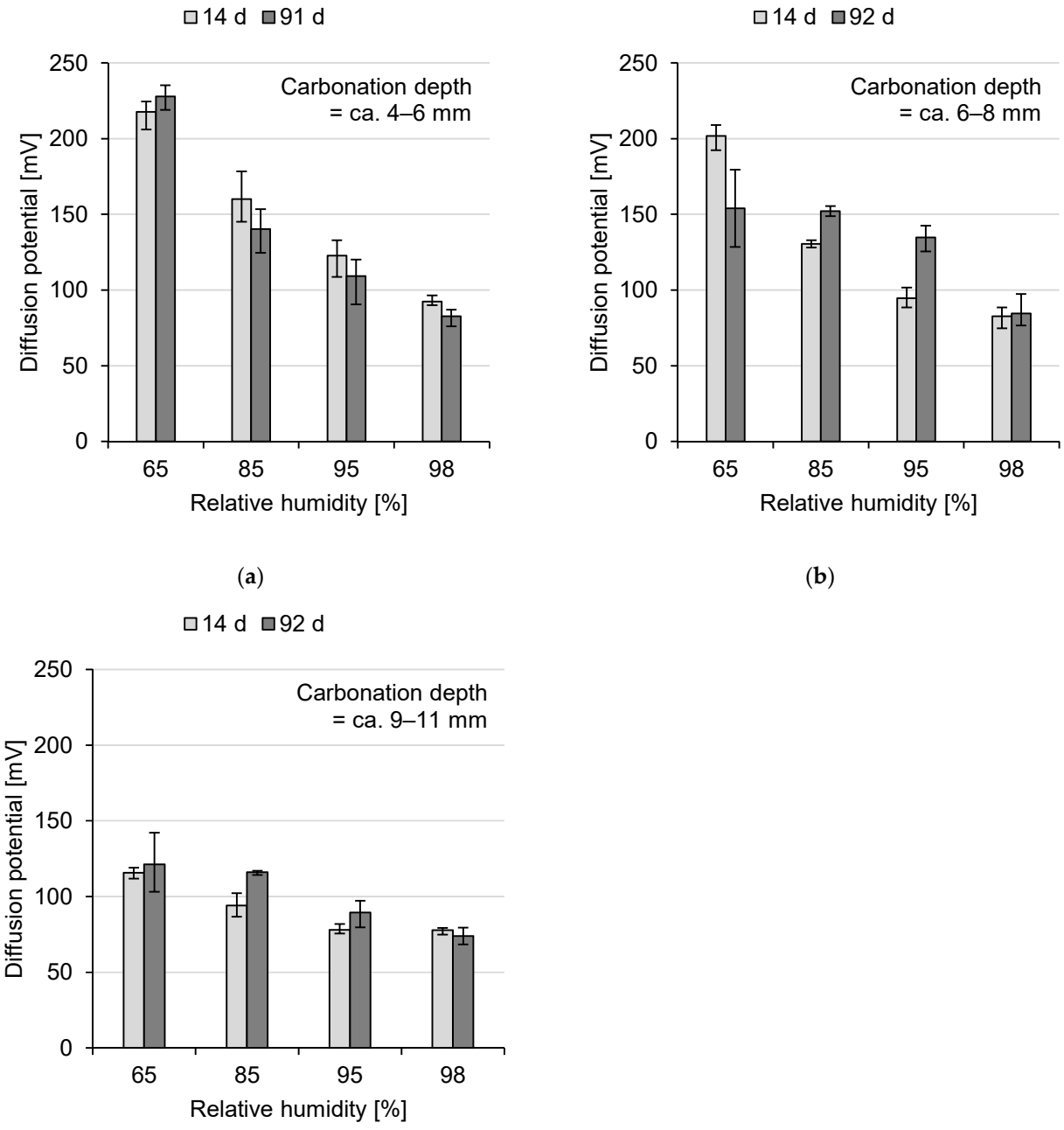

Figure 10. Diffusion potentials in the (**a**) OPC-0.5, (**b**) OPC-0.7, and (**c**) BFC-0.5 mortars after preconditioning at various ambient RHs over two weeks and three months (average, minimum, and maximum value of usually three measurements).

3.5. Performance of the Diffusion Potential Measurement Setup

When measuring diffusion potentials, the performance of the measurement setup has to be examined. The measurement setup in Figure 3 was used for all the diffusion potential measurements in this study. Only the RE coupling solutions changed. Figure 11 plots the diffusion potentials at carbonation depths > 4 mm in the OPC-0.5, OPC-0.7, and BFC-0.5 mortars for the RE coupling 1 (tap water) and RE coupling 2 (sat. KCl solution). This figure shows the measured diffusion potentials in the mortars after preconditioning at various ambient RHs over two weeks, and saturation with water. The diffusion potentials are found to be comparable for most of the mortar moisture conditions. This shows that both RE coupling 1 and RE coupling 2 are suitable for the measurement of diffusion potentials.

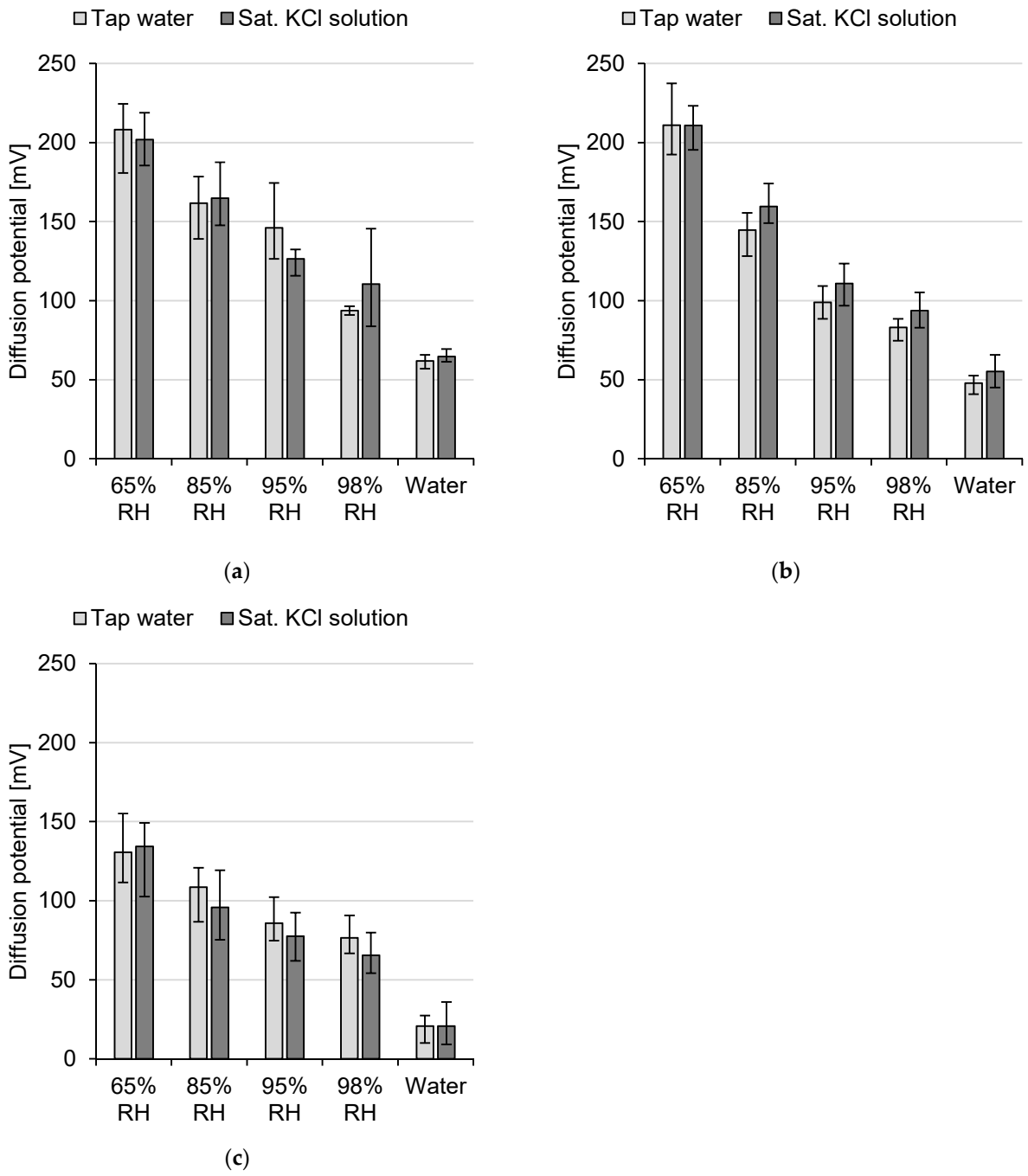

Figure 11. Measured diffusion potentials at carbonation depths > 4 mm in the (**a**) OPC-0.5, (**b**) OPC-0.7, and (**c**) BFC-0.5 mortars after preconditioning at various ambient RHs over two weeks, and saturation with water when using RE coupling 1 and RE coupling 2 (average, minimum, and maximum values).

There was the penetration of the RE coupling agent into the mortar, as can be seen in Figure 12. Figure 12 shows the carbonation depth, visualized with thymolphthalein indicator, and the KCl solution (RE coupling 2), which penetrated the mortar samples during the measurements. After the application of a silver nitrate solution with a concentration of 0.1 M, silver chloride precipitated and indicated the KCl-contaminated areas. Note that the carbonated area does not turn brown when using the silver nitrate method [46]. Despite this, the Cl-contaminated areas slightly differ from the uncontaminated carbonated areas in this study. This suggests that the chloride penetration in carbonated mortar is similar to that of the uncarbonated mortar.

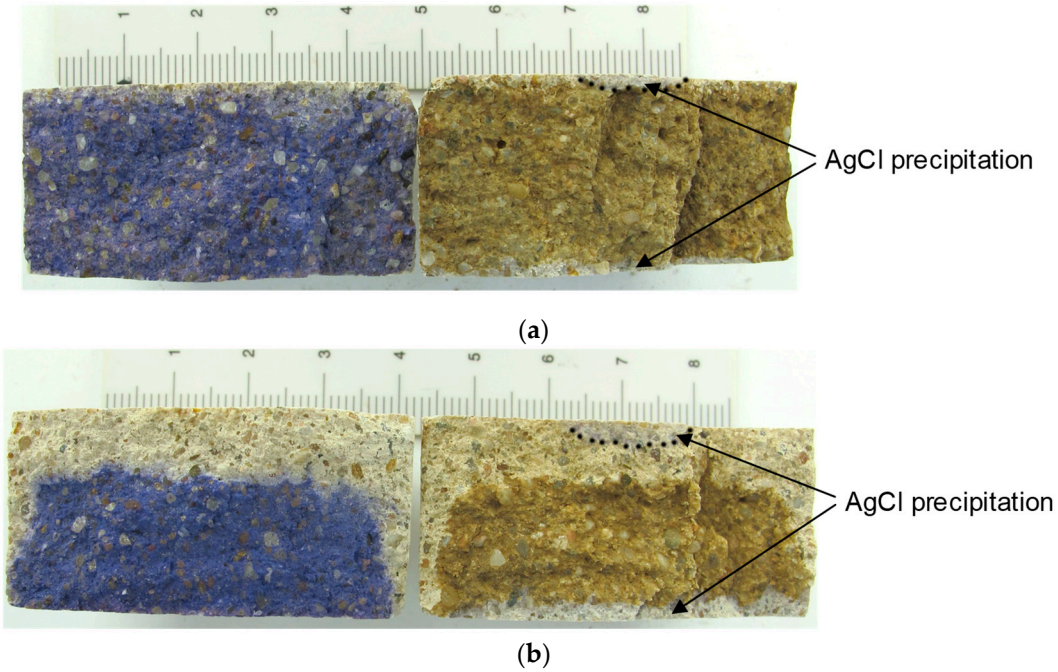

Figure 12. Visual inspection of the carbonation depth and the ingress of the RE coupling agent (saturated KCl solution) after application of thymolphthalein indicator (**left**) and silver nitrate solution (**right**) for (**a**) OPC-0.5 and (**b**) OPC-0.7 mortar samples (cropped images, 15–20% brightening, and the original images are attached; see Supplementary Materials).

It reveals that the KCl coupling solution penetrated the mortar sample to a depth of approx. 2–4 mm. The penetrating RE coupling solution changed the pore solution composition and the moisture condition of the near-surface area in the mortar, which could have particularly affected the measured diffusion potentials at small carbonation depths. For carbonation depths > 2–4 mm, the diffusion potentials can reliably be measured with the introduced setup.

- The diffusion potentials are found to be comparable when using various RE coupling agents (tap water, saturated KCl solution), and the diffusion potentials can reliably be measured with the introduced setup for carbonation depths > 2–4 mm.
- At small carbonation depths < 2–4 mm, however, the RE coupling solution could affect the diffusion potentials in unsaturated mortars, as it changes the pore solution composition and the moisture condition of the near-surface area.

3.6. Diffusion Potentials as Error Source in Corrosion-Related Investigations

This section presents the significance of the diffusion potentials as an error source in half-cell potential measurements, in research and in practice. Since the measured half-cell potentials differ from situation to situation due to numerous influencing factors, such as the concrete moisture condition, the chemical composition of the pore solution (Cl, pH), the oxygen concentration, etc., fundamental considerations are made to give a better understanding of the diffusion potential error when measuring half-cell potentials.

In this research study, the diffusion potentials measure considerable values (up to 240 mV) in cement-based materials with pH differences due to carbonation, particularly at low ambient RHs. It shows that prewetting decreases the magnitude of the diffusion potentials and, therefore, can help to reduce the diffusion potential error in half-cell potential measurements. This is important to pay attention to if single half-cell potential readings are the basis for decisions on the repair of reinforced concrete structures suffering from corrosion. In this case, the diffusion potentials can be a significant source of measurement

errors and must be taken into account. When comparing the measured half-cell potentials next to each other (half-cell potential mapping) or with initial values (corrosion onset monitoring), i.e., considering the size of the potential drop instead of the single potential readings, the situations are as follows.

Half-cell potential mapping: Figure 13a shows half-cell potential mapping on the reinforced concrete structures suffering from chloride-induced steel corrosion. This method is based on the measurement of half-cell potentials when moving an external reference electrode along the concrete surface to localize the areas of actively corroding steel [1]. Steel corrosion is indicated by a notable drop (>150 mV) in the measured half-cell potential (E) [1,47], as can be seen in Figure 13a. If pH differences in the concrete are present, there could be diffusion potentials of up to several hundreds of millivolts depending on the concrete moisture condition, the type of cement, etc., as shown in this study (10–240 mV). The diffusion potentials shift the half-cell potential readings towards more positive values.

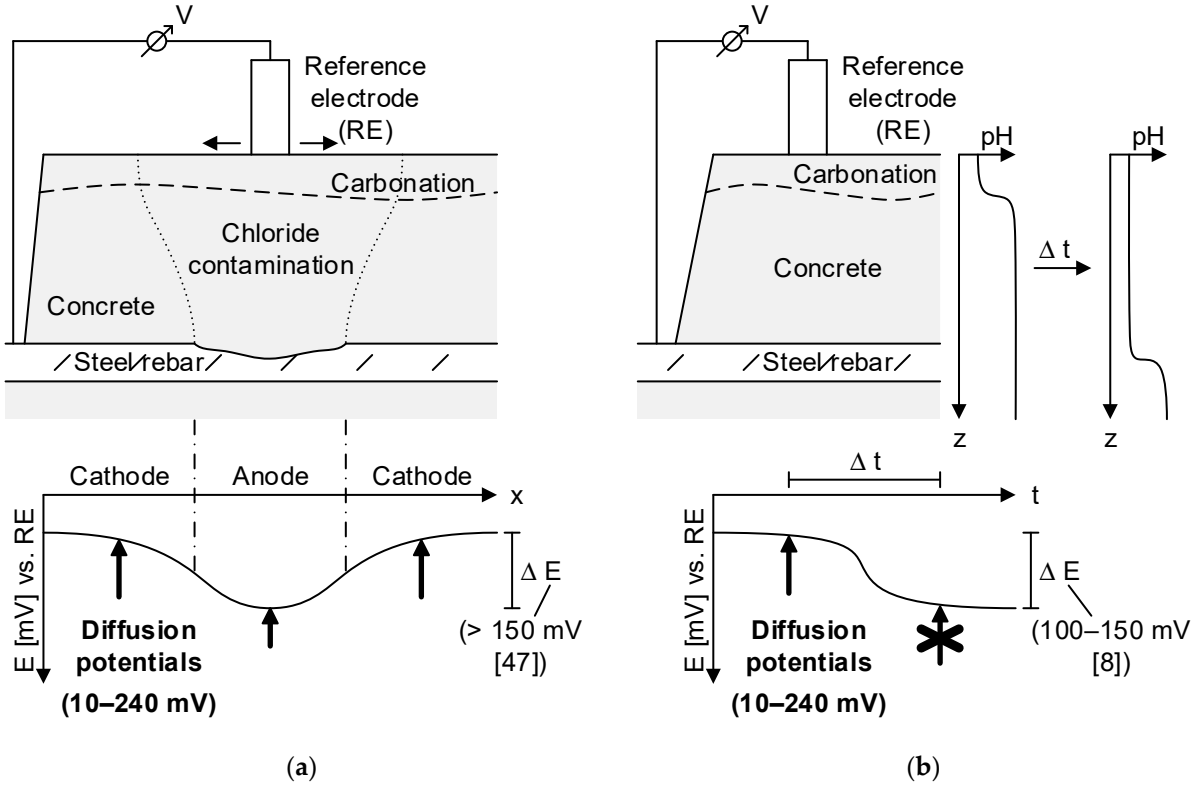

Figure 13. Half-cell potential measurements including the diffusion potentials: (**a**) half-cell potential mapping and (**b**) corrosion onset monitoring.

In the anodic areas, comparably smaller diffusion potentials can be expected due to the presence of chlorides, which presumably increase the ionic conductivity in the carbonated concrete part associated with a diffusion potential depression (compare with [11]). Furthermore, the moisture condition of the chloride-contaminated concrete could be increased [2]. Both of these may considerably decrease the magnitude of the diffusion potentials in the anodic areas and thus the shift of the half-cell potential reading into the positive direction. This would amplify the drop of the measured half-cell potential, which would be beneficial for the localization of the steel corrosion areas. A subsequent study is required to confirm this.

Corrosion onset monitoring: Figure 13b shows the monitoring of the corrosion onset based on the half-cell potential measurements in the case of carbonation-induced steel corrosion. This figure plots the measured half-cell potential (E) over time (t) using an external reference electrode placed on the carbonated concrete surface. As soon as the

carbonation front reaches the steel rebar, the half-cell potential drops towards more negative values (by approx. 100–150 mV in [8]) indicating the initiation of active steel corrosion.

As shown above, the diffusion potentials caused by the pH differences present in concrete make the half-cell potential readings more positive. In a fully carbonated concrete (cover), the pH differences are no longer present, and the diffusion potentials disappear. This has an amplifying effect on the size of the potential drop and, therefore, is beneficial for the detection of corrosion initiation.

- For both half-cell potential mapping and corrosion onset monitoring, the diffusion potentials are not expected to be a significant source of measurement error because the size of the potential drop is considered rather than the single potential readings.

4. Conclusions

This study successfully improves the understanding of the diffusion potentials in cement mortars with pH differences due to carbonation, and their effect on half-cell potential measurements. The following conclusions are drawn:

- The diffusion potentials in the mortars under study have measurement values between 10 and 240 mV. The measured diffusion potentials seem to correlate with the magnitude of the pH drop rather than the progress of the carbonation depth. Furthermore, permselective action presumably has an effect on the arising diffusion potentials.
- The moisture conditions of the mortars significantly affect the magnitude of the resulting diffusion potentials. The higher the diffusion potentials, the lower the ambient RH during the preconditioning of the mortar samples. The magnitude of the diffusion potentials increases by approx. 2–4 mV/% RH for the OPC-0.7 mortar and 1–2 mV/% RH for the BFC-0.5 mortar with decreasing RHs in the studied range of 65–98% at carbonation depths > 3–4 mm. This presumably results from the pore wall interactions, which are expected to be more pronounced at decreased mortar moisture conditions, as only the smaller pores are filled with the pore solution. Further research is necessary.
- The measured diffusion potentials are found to be comparable when using various RE coupling agents (tap water, saturated KCl solution). However, the RE coupling solution penetrates the mortars to a depth of approx. 2–4 mm, which changes the pore solution composition and the moisture condition of the near-surface area in the mortar under study. This could affect the measured diffusion potentials in the unsaturated mortars at small carbonation depths. For carbonation depths > 2–4 mm, the diffusion potentials can reliably be measured with the introduced setup.
- The diffusion potentials in concrete may significantly interfere with the half-cell potential measurements, which indicate steel corrosion through the drop of the half-cell potential. If the potential drop is considered rather than the single potential readings, the diffusion potentials can have an amplifying effect on the size of the potential drop, which is beneficial for the detection of steel corrosion. Therefore, the diffusion potentials are not expected to be a significant source of measurement error for both the half-cell potential mapping and the corrosion onset monitoring.

Last but not least, it has to be mentioned that the half-cell potential measurements have been applied to structures in research and practice. While both concrete and mortar are subject to research projects, the existing structures have often been manufactured of concrete. This requires further research about the diffusion potentials that arise in concrete. In addition to pH differences, chloride concentration differences are usually present, which need to be considered in a subsequent study.

Supplementary Materials: The following supporting information can be downloaded at https://www.mdpi.com/article/10.3390/cmd6010002/s1: data; Figure S1: Original image (Figure 4); Figure S2: Original image (Figure 5 OPC-0.5 28d); Figure S3: Original image (Figure 5 OPC-0.5 84d); Figure S4: Original image (Figure 5 OPC-0.7 28d); Figure S5: Original image (Figure 5 OPC-0.7 56d); Figure S6: Original image (Figure 5 BFC-0.5 28d); Figure S7: Original image (Figure 5 BFC-0.5 42d); Figure S8: Original image (Figure 12a); and Figure S9: Original image (Figure 12b).

Author Contributions: Conceptualization, E.Z. and C.G.; data curation, E.Z.; formal analysis, E.Z. and K.O.; funding acquisition, C.G.; investigation, E.Z.; methodology, E.Z. and C.G.; project administration, E.Z. and K.O.; resources, E.Z.; supervision, K.O. and C.G.; visualization, E.Z.; writing—original draft and editing, E.Z.; writing—review, K.O. and C.G. All authors have read and agreed to the published version of the manuscript.

Funding: This research study was funded by the Deutsche Forschungsgemeinschaft (DFG) (project number 276790461).

Data Availability Statement: The data and original images presented in this study are included in the Supplementary Material. Further inquiries can be directed to the corresponding author.

Acknowledgments: The authors thank the Deutsche Forschungsgemeinschaft (DFG) for the financial support of this research study. We thank Ueli Angst and his team from the Eidgenössische Technische Hochschule in Zurich (ETHZ) for the discussions in this research project.

Conflicts of Interest: The authors declare no conflicts of interest.

References

1. Deutsche Gesellschaft für Zerstörungsfreie Prüfung. *Merkblatt B 03: Merkblatt für Elektrochemische Potentialmessungen zur Detektion von Bewehrungsstahlkorrosion*, 3rd ed.; DGZfP: Berlin, Germany, 2014; ISBN 978-3-940283-10-8.
2. Sodeikat, C.; Gehlen, C.; Schießl, P. Auffinden von Bewehrungskorrosion mit Hilfe der Potentialfeldmessung—Ein ungewöhnlicher Praxisfall. *Beton- u. Stahlbetonbau* **2002**, *97*, 437–444. [CrossRef]
3. Raupach, M.; Schießl, P. Macrocell sensor systems for monitoring of the corrosion risk of the reinforcement in concrete structures. *NDTE Int.* **2001**, *34*, 435–442. [CrossRef]
4. Angst, U.M.; Elsener, B.; Larsen, C.K.; Vennesland, Ø. Chloride induced reinforcement corrosion: Electrochemical monitoring of initiation stage and chloride threshold values. *Corros. Sci.* **2011**, *53*, 1451–1464. [CrossRef]
5. Boubitsas, D.; Tang, L. The influence of reinforcement steel surface condition on initiation of chloride induced corrosion. *Mater. Struct.* **2015**, *48*, 2641–2658. [CrossRef]
6. Scott, A.; Alexander, M.G. Effect of supplementary cementitious materials (binder type) on the pore solution chemistry and the corrosion of steel in alkaline environments. *Cem. Concr. Res.* **2016**, *89*, 45–55. [CrossRef]
7. Williamson, J.; Isgor, O.B. The effect of simulated concrete pore solution composition and chlorides on the electronic properties of passive films on carbon steel rebar. *Corros. Sci.* **2016**, *106*, 82–95. [CrossRef]
8. Belda Revert, A.; De Weerdt, K.; Hornbostel, K.; Geiker, M.R. Carbonation-induced corrosion: Investigation of the corrosion onset. *Constr. Build. Mater.* **2018**, *162*, 847–856. [CrossRef]
9. Myrdal, R. Phenomena that disturb the measurement of potentials in concrete. In Proceedings of the NACE International Corrosion Conference, Denver, CO, USA, 24–29 March 1996; p. 339.
10. Angst, U.; Vennesland, Ø.; Myrdal, R. Diffusion potentials as source of error in electrochemical measurements in concrete. *Mater. Struct.* **2009**, *42*, 365–375. [CrossRef]
11. Angst, U.; Vennesland, Ø. Detecting critical chloride content in concrete using embedded ion selective electrodes—Effect of liquid junction and membrane potentials. *Mater. Corros.* **2009**, *60*, 638–643. [CrossRef]
12. Büchler, M.; Schiegg, Y. *Investigation Regarding the Potential Mapping on Reinforced Concrete Structures*; Report 634; Swiss Society for Corrosion Protection: Zurich, Switzerland, 2008. (In German)
13. Angst, U.; Elsener, B.; Myrdal, R.; Vennesland, Ø. Diffusion potentials in porous mortar in a moisture state below saturation. *Electrochim. Acta* **2010**, *55*, 8545–8555. [CrossRef]
14. Angst, U.; Elsener, B.; Larsen, C.K.; Vennesland, Ø. Potentiometric determination of the chloride ion activity in cement based materials. *J. Appl. Electrochem.* **2010**, *40*, 561–573. [CrossRef]
15. Zhang, J.-Z.; Li, J.Y.; Buenfeld, N.R. Measurement and modelling of membrane potentials across OPC mortar specimens between 0.5 M NaCl and simulated pore solutions. *Cem. Concr. Compos.* **2002**, *24*, 451–455. [CrossRef]

16. Bard, A.J.; Faulkner, L.R. *Electrochemical Methods—Fundamentals and Applications*, 2nd ed.; Wiley: New York, NY, USA, 2001; ISBN 978-0471043720.
17. Anstice, D.J.; Page, C.L.; Page, M.M. The pore solution phase of carbonated cement pastes. *Cem. Concr. Res.* **2005**, *35*, 377–383. [CrossRef]
18. McPolin, D.O.; Basheer, P.A.M.; Long, A.E. Carbonation and pH in Mortars Manufactured with Supplementary Cementitious Materials. *J. Mater. Civ. Eng.* **2009**, *21*, 217–225. [CrossRef]
19. Pu, Q.; Jiang, L.; Xu, J.; Chu, H.; Xu, Y.; Zhang, Y. Evolution of pH and chemical composition of pore solution in carbonated concrete. *Constr. Build. Mater.* **2012**, *28*, 519–524. [CrossRef]
20. Hren, M.; Kosec, T.; Legat, A.; Bokan-Bosiljkov, V. Corrosion performance of steel in blended cement pore solutions. *Mater. Technol.* **2019**, *53*, 679–686. [CrossRef]
21. Liu, X.; Niu, D.; Li, X.; Lv, Y.; Fu, Q. Pore Solution pH for the Corrosion Initiation of Rebars Embedded in Concrete under a Long-Term Natural Carbonation Reaction. *Appl. Sci.* **2018**, *8*, 128. [CrossRef]
22. Nedeljković, M.; Ghiassi, B.; van der Laan, S.; Li, Z.; Ye, G. Effect of curing conditions on the pore solution and carbonation resistance of alkali-activated fly ash and slag pastes. *Cem. Concr. Res.* **2019**, *116*, 146–158. [CrossRef]
23. Cascudo, O.; Pires, P.; Carasek, H.; de Castro, A.; Lopes, A. Evaluation of the pore solution of concretes with mineral additions subjected to 14 years of natural carbonation. *Cem. Concr. Compos.* **2021**, *115*, 103858. [CrossRef]
24. Chen, L.; Tian, Z.; Zhu, Z.; Su, R.K.L. Effects of carbonation and sponge wetting solution on diffusion potential of carbonated concrete with suppplementary cementitious materials. *Constr. Build. Mater.* **2024**, *430*, 136490. [CrossRef]
25. Stark, J.; Wicht, B. *Dauerhaftigkeit von Beton*, 2nd ed.; Springer: Heidelberg, Germany, 2013; ISBN 978-3-642-35278-2.
26. Ziehensack, E.; Keßler, S.; Angst, U.; Hilbig, H.; Gehlen, C. Diffusion potentials in saturated hardened cement paste upon chloride exposure. *Mater. Struct.* **2023**, *56*, 100. [CrossRef]
27. *DIN EN 196-1:2016-11*; Methods of Testing Cement—Part 1: Determination of Strength. Beuth Verlag: Berlin, Germany, 2016. (In German)
28. *DIN EN 12390-12:2020-04*; Testing Hardened Concrete—Part 12: Determination of the Carbonation Resistance of Concrete—Acceleratred Carbonation Method. Beuth Verlag: Berlin, Germany, 2020. (In German)
29. Schulte Holthausen, R.; Raupach, M. Monitoring the internal swelling in cementitious mortars with single-sided ^{1}H nuclear magnetic resonance. *Cem. Concr. Res.* **2018**, *111*, 138–146. [CrossRef]
30. Mengel, L.; Krauss, H.-W.; Lowke, D. Water transport through cracks in plain and reinforced concrete—Influencing factors and open questions. *Constr. Build. Mater.* **2020**, *254*, 118990. [CrossRef]
31. Rucker-Gramm, P. Modellierung des Feuchte- und Salztransports unter Berücksichtigung der Selbstabdichtung in Zementgebundenen Baustoffen. Ph.D. Thesis, Technische Universität München, München, Germany, 2008.
32. Boguszynska, J.; Brown, M.C.A.; McDonald, P.J.; Mitchell, J.; Mulheron, M.; Tritt-Goc, J.; Verganelakis, D.A. Magnetic resonance studies of cement based materials in inhomogeneous magnetic fields. *Cem. Concr. Res.* **2005**, *35*, 2033–2040. [CrossRef]
33. Van Landeghem, M.; d'Espinose de Lacaillerie, J.-B.; Blümich, B.; Korb, J.-P.; Bresson, B. The roles of hydration and evaporation during the drying of a cement paste by localized NMR. *Cem. Concr. Res.* **2013**, *48*, 86–96. [CrossRef]
34. Zhaxi, Q.; Zhou, H.; Long, Z.; Guo, J.; Zhou, Y.; Zhang, Z. Nondestructive Measurement of the Water Content in Building Materials by Single-Sided NMR-MOUSE. *Sustainability* **2023**, *15*, 11096. [CrossRef]
35. ACT GmbH (Ed.) *Profile NMR-MOUSE PM 25*; Technical data sheet; ACT GmbH: Aachen, Germany, 2010.
36. Ahlborn Mess- und Regelungstechnik GmbH (Ed.) *ALMEMO Precision Measurement Devices*; Technical data sheet; Ahlborn Mess- und Regelungstechnik GmbH: Holzkirchen, Germany, 2021.
37. Stadtwerke München (Ed.) *Münchner Trinkwasser-Analysewerte (Stand: Januar 2023)*; Report; Stadtwerke München: München, Germany, 2023.
38. Kakiuchi, T. Salt bridge in electroanalytical chemistry: Past, present, and future. *J. Solid State Electrochem.* **2011**, *15*, 1661–1671. [CrossRef]
39. De Weerdt, K.; Plusquellec, G.; Belda Revert, A.; Geiker, M.R.; Lothenbach, B. Effect of carbonation on the pore solution of mortar. *Cem. Concr. Res.* **2019**, *118*, 38–59. [CrossRef]
40. Lide, D.R. (Ed.) *CRC Handbook of Chemistry and Physics*, 85th ed.; CRC Press: Boca Raton, FL, USA, 2004; ISBN 978-0849304859.
41. Germann Instruments (Ed.) *Deep Purple and Rainbow Indicators*; Technical data sheet; Germann Instruments: Copenhagen, Denmark, 2024.
42. Lydzba, D.; Rajczakowska, M.; Stefaniuk, D.; Kmita, A. Identification of the carbonation zone in concrete using x-ray microtomography. *Stud. Geotech. Mech.* **2014**, *36*, 47–54. [CrossRef]
43. Benzecry, V.; Al-Khafaji, A.F.; Haluza, R.T.; Bakis, C.E.; Myers, J.J.; Nanni, A. Durability Assessment of 15- to 20-Year-Old GFRP Bars Extracted from Bridges in the US. I: Selected Bridges, Bar Extraction, and Concrete Assessment. *J. Compos. Constr.* **2021**, *25*, 04021007. [CrossRef]

44. Diaz Caselles, L.; Cau Dit Coumes, C.; Antonucci, P.; Rousselet, A.; Mesbah, A.; Montouillout, V. Chemical degradation of magnesium potassium phosphate cement pastes during leaching by demineralized water: Experimental investigation and modeling. *Cem. Concr. Res.* **2024**, *178*, 107456. [CrossRef]
45. Thiel, C. Einfluss von CO_2-Druck und Feuchtegehalt auf das Porengefüge von Zementgebundenen Materialien während der Carbonatisierung. Ph.D. Thesis, Technische Universität München, München, Germany, 2023.
46. Pontes, C.V.; Réus, G.C.; Araújo, E.C.; Medeiros, M.H.F. Silver nitrate colorimetric method to detect chloride penetration in carbonated concrete: How to prevent false positives. *J. Build. Eng.* **2021**, *34*, 101860. [CrossRef]
47. Tang, L.; Frederiksen, J.M.; Angst, U.M.; Polder, R.; Alonso, M.C.; Elsener, B.; Hooton, R.D.; Pacheco, J. Experiences from RILEM TC 235-CTC in recommending a test method for chloride threshold values in concrete. *RILEM Tech. Lett.* **2018**, *3*, 25–31. [CrossRef]